2011

# Length of the annular regime for condensing flows inside a horizontal channel - the experimental determination of its values and its trends

Patcharapol Gorgitrattanagul
*Michigan Technological University*

# THE LENGTH OF THE ANNULAR REGIME FOR CONDENSING FLOWS INSIDE A HORIZONTAL CHANNEL - THE EXPERIMENTAL DETERMINATION OF ITS VALUES AND ITS TRENDS

By

Patcharapol Gorgitrattanagul

A THESIS

Submitted in partial fulfillment of the requirements for the degree of

MASTER OF SCIENCE

(Mechanical Engineering)

MICHIGAN TECHNOLOGICAL UNIVERSITY

2011

This thesis, “The Length of The Annular Regime for Condensing Flows Inside A Horizontal Channel - The Experimental Determination of Its Values and Its Trends,” is hereby approved in partial fulfillment of the requirements for the Degree of MASTER OF SCIENCE IN MECHANICAL ENGINEERING.

Department of Mechanical Engineering-Engineering Mechanics

Signatures:

Thesis Advisor _____

Amitabh Narain

Committee Member _____

Allan A. Struthers

Committee Member _____

Charles H. Margraves

Committee Member _____

Dennis DeSheng Meng

Department Chair _____

William W. Predebon

Date _____

# TABLE OF CONTENTS

## LIST OF FIGURES

## LIST OF TABLES

# Acknowledgements

First of all, I am grateful to the government of Thailand for financially supporting my graduate education in the U.S.

I am also thankful to my advisor, Dr. Amitabh Narain, for his mentoring, guidance and support.

Next my gratitude goes to Michael T. Kivisalu, a fellow graduate student, who taught guided, and helped me during my study at Michigan Technological University. He never gets tired of teaching me the same thing multiple times.

I am grateful to my many friends for giving me a great life outside of school and also helping me as co-learners in many of my academic assignments.

My parents come last but they are the most important. Without their guidance and support, I would not have the chance to mature as an individual. Furthermore, without their encouragement, my pursuit of a graduate education away from home would not have been possible. This thesis is dedicated to them for their superb support throughout my entire life.

## Nomenclature

| | |
|---|---|
| $\dot{M}_{in}$ | Inlet mass flow rate to the test-section, g/s |
| $\Delta T$ | $T_{sat}$ - $\overline{T}_w$ , °C |
| $X_A$ | The length of annular regime, cm |
| h | Channel height, mm |
| $K_l$ | Conductivity of condensate liquid, W/(m·K) |
| $\overline{T}_w$ | Average temperature of condenser surface, °C |
| $T_{sat}$ | Saturation temperature vapor at test-section inlet, °C |
| $C_{pl}$ | Specific heat of the liquid condensate, J/(kg·K) |
| $K_l$ | Thermal conductivity, W/(m·K) |
| $\mu$ | Fluid viscosity, kg/(m·s) |
| $\rho$ | Fluid density, kg/m$^3$ |
| $q''$ | Heat-flux, W/cm$^2$ |
| $p_{in}$ | Pressure at the test-section inlet, kPa |
| $P_{exit}$ | Pressure at the test-section exit, kPa |
| $\Delta p$ | $p_{in}$ - $p_{exit}$ , kPa |
| $h_{fg}$ | Enthalpy of vaporization, kJ/kg |
| $Re_{in}$ | Inlet vapor Reynolds number, $\rho_2 Ud/\mu_2$ |
| $Pr_l$ | Prandlt number of condensate, $\mu_1 \cdot C_{pl}/k_1$ |
| Ja | Condensate liquid Jakob number, $C_{pl} \cdot \Delta T/h_{fg}$ |
| PID | Proportional-integral-derivative of feedback control |
| TEC | Solid state heat pump |

## Subscript

| | |
|---|---|
| 1 | Liquid phase |
| 2 | Vapor phase |
| A | Annular |
| Exit | Test-section exit |
| In | Test-section inlet |
| Sat | Saturation |
| W | Wall/condensing surface |

## ABSTRACT

The experiments observe and measure the length of the annular regime in fully condensing quasi-steady (steady-in-the-mean) flows of pure FC-72 vapor in a horizontal condenser (rectangular cross-section of 2 mm height, 15 mm width, and 1 m length). The sides and top of the duct are made of clear plastic that allows flow visualization. The experimental system in which this condenser is used is able to control and achieve different quasi-steady mass flow rates, inlet pressures, and wall cooling conditions (by adjustment of the temperature and flow rate of the cooling water flowing underneath the condensing-plate). The reported correlations and measurements for the annular length are also vital information for determining the length of the annular regime and proposing extended correlation (covering many vapors and a larger parameter set than the experimentally reported version here) by ongoing independent modeling and computational simulation approach.

# 1. Introduction

For pressure/shear driven internal condensing flows, this thesis presents fundamental experimental measurements of the length of its annular regime. The dependence of this length on the incoming vapor mass flow rate and the rate of cooling (imposed on the condensing-surface) is also investigated. The experimental results reported here are important for a meaningful assessment of such a shear driven condenser's performance in any closed flow loop facility, be it an experimental facility or a system of practical interest, as well as to help design new systems that plan to maintain all annular and partially condensing flow regimes inside the condenser.

Shear/pressure driven internal condensing flows are of interest here because they occur in horizontal ducts, micro-gravity, and micro-meter scale hydraulic diameter ducts of interest to next generation space based thermal management systems and high heat-flux electronic cooling systems.

There are many experimental papers that deal with the condensation of pure vapors flowing inside vertical or horizontal ducts (of circular or rectangular cross-sections, as in (Goodykoontz and Dorsch 1966; Cavallini and Zechchin 1971). The experiments as well as related correlations (Shah 1979; Cavallini et al. 1974) in the literature cover a large set of flow regimes and associated flow physics categories, see also (Mitra et al. 2011; Kurita et al. 2011). Despite this they are known experimental works that do not measure the length of the annular regime.

Note that, as shown in (Kurita et al. 2011), gravity driven condensing flows are almost always annular. However, shear/pressure driven fully condensing flows' quasi-steady realization under quasi-steady prescriptions of mean inlet mass flow rate, the mean inlet pressures, and cooling conditions often lead to thermally inefficient non-annular regimes (plug-slug, bubbly, etc.) from a certain distance onward. Since this distance can be small or large, this work establishes experimentally observed trends of changes in annular length with respect to total inlet mass flow rate, $\dot{M}_{in}$, and temperature difference between the vapor and the condensing-surface, $\Delta T$.

The unique sensitivities of such flows' heat transfer rates to inadvertent or deliberate impositions of fluctuations/pulsations on the mean values are also important, see (Kivisalu et al. 2011a; Kivisalu et al. 2011b), but are not part of the reported investigations. For the reported investigations, externally imposed pressure-difference fluctuations are negligible.

The reported results advance prediction capabilities for shear/pressure driven internal condensing flows (in micro-gravity or micro-scale ducts) by supporting ongoing computational simulation works that deal with prediction of the length of the annular regime as well as the heat-flux performance of the annular regime. New computational results for the reported quasi-steady shear/pressure driven condensing flows experiments will be reported elsewhere and are not part of this thesis.

In conclusion, the reported experimental results advance the quest for a well understood and repeatable definition of the parameter space boundaries within which annular shear/pressure driven flows can be realized.

# 2. Experimental Set -Up

## 2.1 Description

Fully condensing flows of FC-72 vapor in a horizontal rectangular duct (2 mm high, 15 mm wide and 1 m long) are investigated (see Fig.2.1). Its horizontal condensing surface area (15 mm x 1 m) is the top of a 12.7 mm thick stainless steel plate. The top and side surfaces of the channel are made of a transparent material (Laxen), which is covered with an insulation that can be removed to allow flow visualization while the system is running.

This condenser is part of a flow loop which is schematically depicted in Fig. 2.2 and this flow-loop's actual photograph is shown in Fig. 2.3

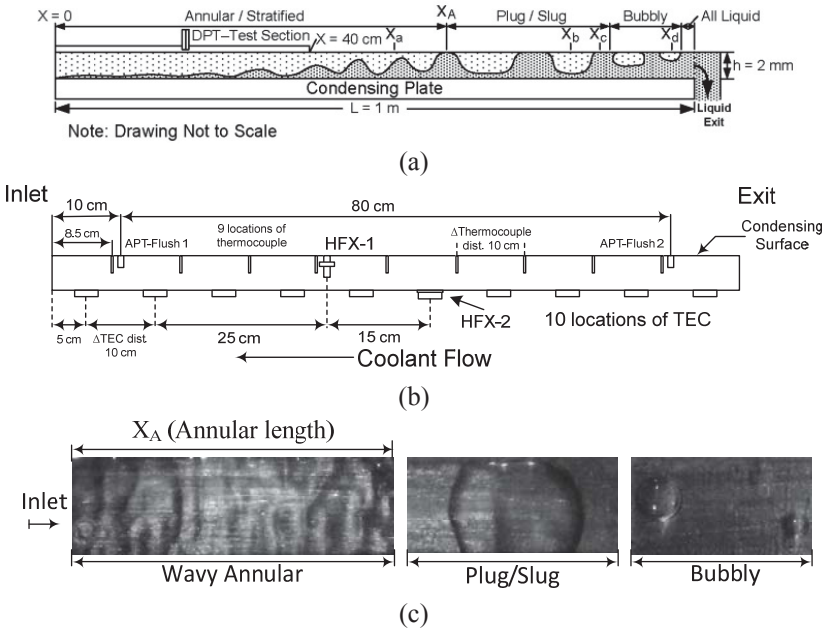


Fig. 2.1: Side views of: (a) the test-section, (b) the instrumented condensing plate (12.7 mm thick steel), and (c) the photograph of actual flow regime

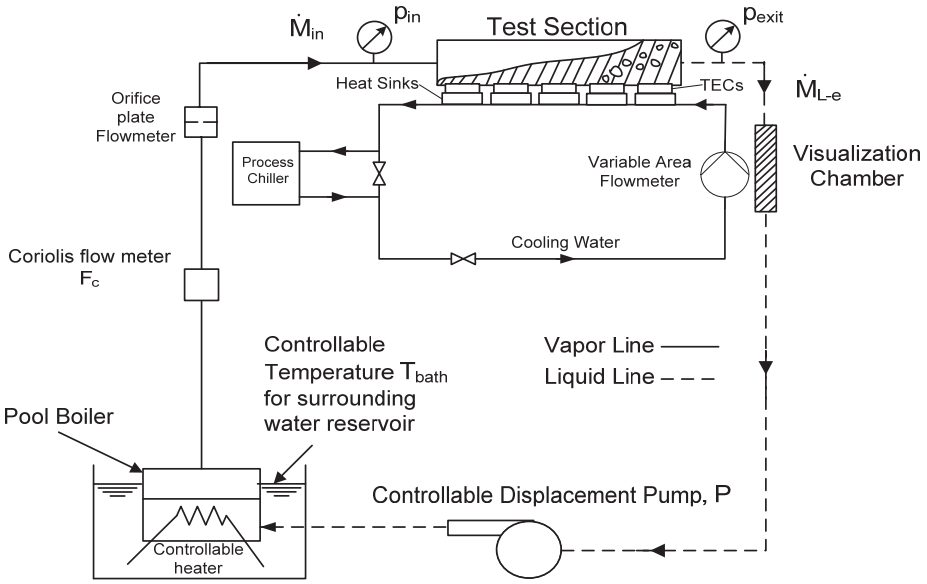


Fig. 2.2: Schematic of the flow-loop which incorporates the test-section

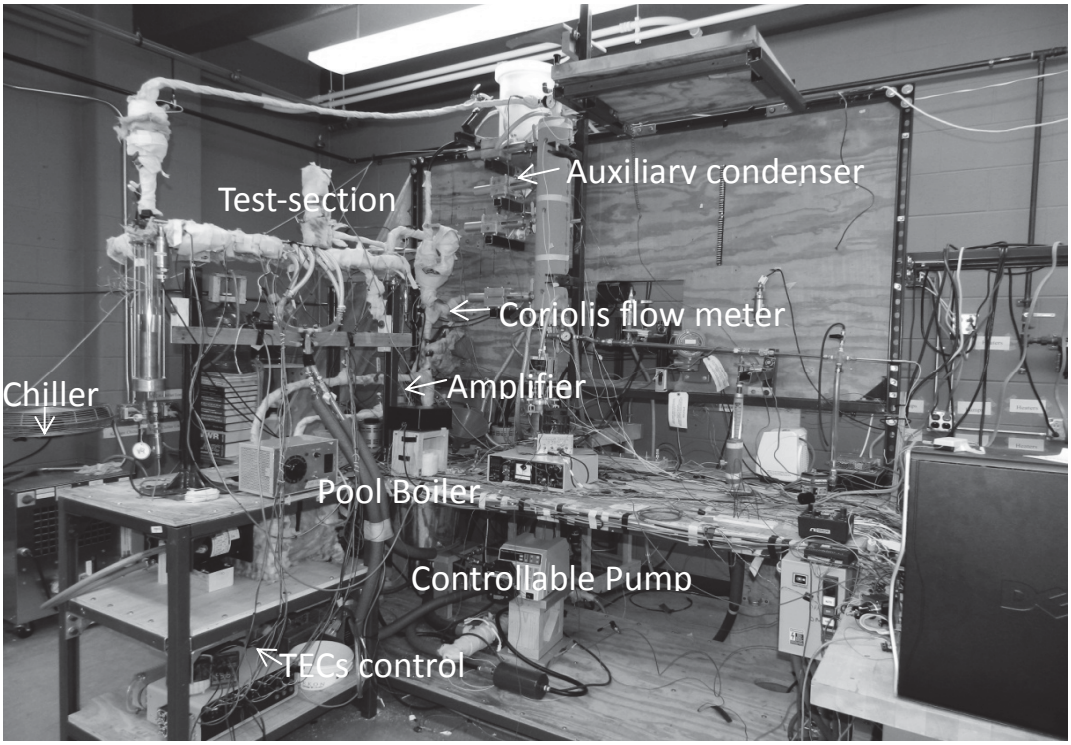


Fig. 2.3: The actual experimental system

The transport and thermodynamic fluid properties of FC-72 were acquired from 3M Corporation. This choice of fluid is for safety of operations under laboratory conditions at a university. The flow loop in Fig. 2.2 has three independent feedback control strategies that can fix steady-in-the-mean values of: inlet mass flow rate, $\dot{M}_{in}$, condensing-surface cooling conditions, and inlet pressure $\overline{p}_{in}$. Mean inlet mass flow rate, $\dot{M}_{in}$, is fixed through active feedback control of the power input to the electric heater inside the pool boiler. The pool boiler pressure is stabilized using the surrounding water reservoir temperature. The condensing-surface temperature, $T_W(x)$, is obtained for a fully specified steady cooling approach that results from a specified water flow rate and temperature of the flow at a specify cross-section. This occurs at the location where the flowing coolant water first approaches the condenser plate. The active feedback control displacement pump, P, is used to fix the inlet pressure, $p_{in}$, of the test-section.

The vapor mass flow rate from the pool boiler $\dot{M}_{in}$ goes into the test-section and is measured by a Coriolis flow meter, $F_c$. This $F_c$ value is controlled by a feedback controlled heater in the pool boiler. The flow of coolant water in Fig. 2.2, see also (Kurita et al. 2011), is supplied with the help of a commercially available process chiller and a manually adjusted value of the water flow rate (0 – 17 liters/min). In addition, as shown in Fig. 2.1b, various Thermo-Electric-Coolers (TECs) are located in the condensing plate. Each of the TECs can be separately activated and controlled for any additional cooling need. However, in this reported experiments these TECs are not used.

## 2.2 Instrumentation

Kulite flush-type, absolute pressure-transducers are used in the test-section at 10 and 90 cm downstream from the inlet of the test-section. Their accuracies, after calibration, are ± 0.7 kPa. Two high accuracy pressure transducers from Omega Engineering are used to measure upstream and downstream pressures for inlet and the exit of the test-section. Their accuracies, after calibration, are ± 0.2 kPa. The accuracies of the other pressure transducers in the system are approximately ± 0.6 kPa. The variable-reluctance type differential pressure transducer used for the test-section, across locations shown in Fig. 2.1a, is from Validyne Inc. It has an after calibration accuracy of ± 20 Pa. Temperatures are measured by T-type thermocouples with accuracies, after calibration, lying within ± 1$^{o}$C. The heat-flux meter from Vatell Corporation, HFX-1 in Fig. 2.1b has an accuracy of approximately ± 7.2% of its reading, in W/cm$^2$, and an approximate range of 0-10 W/cm$^2$ when used with our existing amplifier and data acquisition system. The mean mass flow rate measured from the Coriolis flow meter, $F_c$, in Fig. 2.2 is accurate up to ± 0.35% of flow, or within ±0.007 g/s for the ranges of flow rate (0.4-3.5 g/s) investigated here.

The National Instruments' (NI's) data acquisition system is used to record the mean quasi-steady data of all variables at 1second intervals over the experiments. The data acquisition devices used to acquire data at 1second intervals and run the feedback controls are from National Instruments, see (Kivisalu et al. 2011a) for additional details.

## 2.3 Cooling Condition

The condensing surface's "cooling approach" (which defines its thermal boundary condition) consists of cooling water which flows through the heat removal blocks underneath the 12.7 mm thick condensing plate at a controlled steady flow rate (approximately 8.3 liters per minute) and a controlled temperature (15 - 16 $^{o}$C) as it enters the first cooling block.

The above described cooling approach (with the TECs being off) defines the condensing-surface thermal boundary conditions.

## 2.4 Procedures

2.4.1 Quasi-Steady Flows

The procedure is for achieving steady/quasi-steady fully condensing flows, without exit-imposed fluctuations, and whose effective point of full condensation is within the test-section. Downstream of the exit (including the "Visualization Chamber" in Fig. 2.2), the flow loop is all liquid up to the pool boiler. This procedure involves: (i) fixing the pool boiler bath temperature $T_{bath}$, (ii) holding fixed the mean Coriolis mass flow meter, $F_C$ (in Fig. 2.2) reading of the mass flow rate, $\dot{M}_{in}$, by a PID control of the pool boiler heater, (iii) steadying the condensing-surface temperature, $T_W(x)$, with the help of the cooling approach described in section 2.3, and (iv) using the controllable displacement pump P, through a PID control, to hold the mean inlet pressure fixed at $p_{in} = p_{in}^*$. This procedure allows the exit pressure, $p_{exit}$, to freely seek its natural steady value, $p_{exit}|_{Na}$, to define the natural quasi-steady flow as one with a self-sought pressure-difference $\Delta p|_{Na} = p_{in}^* - p_{exit}|_{Na} \equiv \Delta p|_{N\text{-}F}$ under negligible to insignificant externally imposed fluctuations on vapor flow at the inlet

2.4.2 The Experiment's Hypothesis and the Acquired Data Set

For each quasi-steady flow that was realized, the quasi-steady conditions were maintained for approximately 30-45 minutes. The length of the annular regime, $X_A$, was defined as the time-averaged mean of the distance $X_A(t)$ – which is the distance from the inlet to the point where the liquid first touches the top transparent wall, see Fig. 2.1a.

For the recorded condensing-surface temperature variation, $T_w(x)$, (with its mean $\overline{T}_w(x) \equiv \frac{1}{X_A}\int_0^{X_A} T_w(x)\cdot dx$ ), the non-dimensional temperature, $\theta(x/X_A)$, is defined as

$$\theta(x/X_A) \equiv \frac{T_{sat}(p_{in}) - T_w(x)}{T_{sat}(p_{in}) - \overline{T}_w} \quad . \tag{1}$$

For a fixed cooling approach it is expected and found that $\theta(x/X_A)$ is approximately the same function for different steady realization cases under these conditions, from the modeling and formulation for such internal condition flow problems, see (Mitra et al. 2011; Narain et al. 2004), it is clear that the length of the annular regime, $X_A$,(for these quasi-steady condensing flows of FC-72) can be said to have the following dependence

$$X_A = \text{function}\,(\dot{M}_{in}, \Delta T)\,, \tag{2}$$

where $\dot{M}_{in}$ is the steady mass flow rate of the vapor measured by the Coriolis flow meter, $F_c$, and $\Delta T \equiv T_{sat}(p_{in}) - \overline{T}_w$ is the controlling temperature difference. Here it should be noted that, although the incoming vapor's temperature is 5-10°C above the saturation temperature, $T_{sat}(p_{in})$, the flow is effectively the same as one that would take place if the vapor was at $T_{sat}(p_{in})$. This is a well known behavior, see (Mitra et al. 2011), which results from the fact that in the energy balance at the vapor-liquid interface, heat flow from the vapor is small compared to the latent heat and heat carried away by the liquid (the liquid has much higher conductivity than the vapor).

To experimentally determine the unknown function appearing on the right side of Eq. (2), its arguments $\dot{M}_{in}$ and $\Delta T$ are varied in three sets denoted as set $S_1$, $S_2$, and $S_3$. These sets are shown as curves $S_1$, $S_2$, and $S_3$ in the schematic of Fig. 2.4

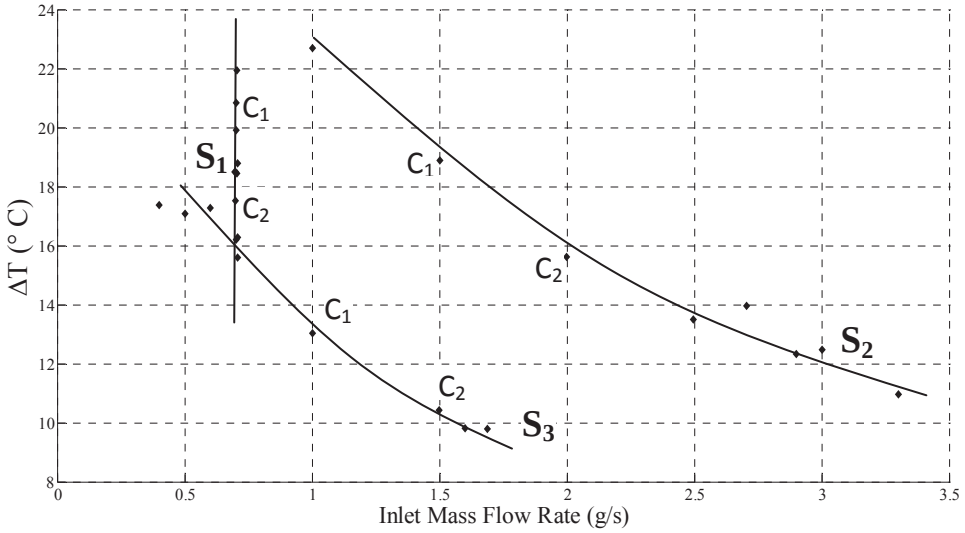


Fig. 2.4: The variation strategies for $\dot{M}_{in}$ and $\Delta T$

Data set $S_1$ was acquired by fixing the inlet mass flow rate, $\dot{M}_{in}$, at approximately 0.7 g/s and varying the test-section inlet pressure, $p_{in}$, to achieve different $\Delta T$ values. The upper and lower limits of $\Delta T$ resulted from the experimentally feasible range of allowed inlet pressure variations. For example, one could not go below a certain sub-atmospheric pressure value of inlet pressure $p_{in}$, because the test-section would leak and suck non-condensable air into the flow. Individual experimental cases along the curve $S_1$ in Fig. 2.4 are denoted as $C_1$, $C_2$, $C_3$, etc. and are reported in Table 4.1 and 4.2 as S1C1, S1C2, S1C3, etc.

Data sets $S_2$ and $S_3$ were acquired by fixing the test-section pressure, $p_{in}$, at 190 kPa and 100 kPa respectively, and subsequently varying the mass flow rate. Note that 190 kPa and 100 kPa are the highest and lowest feasible values of inlet pressure allowed by the design of the test-section and its instruments (pressure transducers). The correlation curves $S_2$ and $S_3$ in Fig. 2.4 tend downwards because, as $\dot{M}_{in}$ increases for a fixed cooling approach, the condensate thins and increases the heat flux through the condensing plate. As a result, the average condensing-surface temperature, $\overline{T}_w$, increases and the value of $\Delta T$ decreases. This causes the curves $S_2$ and $S_3$ to slope downwards.

Individual experimental cases along the curves $S_2$ and $S_3$ in Fig. 2.4 are also denoted by $C_1$, $C_2$, $C_3$, etc. but the cases reported in Tables 4.1 and 4.2 are denoted as: S2C1, S2C2, S2C3 etc. for the Curve/Set associate with $S_2$ and S3C1, S3C2, S3C3, etc. for the Curve/Set associate with $S_3$.

## 3. The non-dimensional version of the hypothesis.

In section 2.4.2, via eq. (2), the dependence hypothesis was stated as

$$X_A = \text{function}\,(\dot{M}_{in}, \Delta T). \tag{3}$$

The objective was to determine the unknown function on the right-side of eq. (2). If one were to look at the modeling/theoretical formulation approach in (Mitra et al. 2011; Narain et al. 2004), it is straight forward to see that, in addition to the argument list in eq. (3), the value of $X_A$ depends on the fluid (i.e. relevant fluid properties appearing in the governing equations), the geometry of the channel, the inlet pressure $p_{in}$ (which determines the saturation temperature, $T_{sat}(p_{in})$), and the cooling condition (as measured by $\theta(x/X_A)$ in eq. (1)). The relevant fluid properties of density, viscosity, specific heat, and thermal conductivity denoted by $\rho$, $\mu$, $C_p$, and k are relatively constant. The subscripts "1" for the liquid phase and "2" for the vapor phase. The channel geometry is defined by its gap height; the channel width "w" does not directly appear in the one-dimensional model and value of latent heat (J/kg) released at the interface is almost constant and is defined by $h_{fg} \cong h_{fg}(T_{sat}(p_{in}))$. Since $\theta(x/X_A)$ is approximately constant, eq. (3) is more completely stated as

$$X_A = \text{function}\,(\dot{M}_{in}, \Delta T; C_{p1}, \rho_1, \mu_1, k_1, h_{fg}, \rho_2, \mu_2, p_{in}, h) \tag{4}$$

Using the Pi-Theorem, (Muson et al. 2009), or using the non-dimensionlization of the governing equations in (Mitra et al. 2011; Narain et al. 2004), one arrives at the following non-dimension form of eq. (4)

$$\frac{X_A}{h} = \text{function}\,(Re_{in}, Ja; \frac{\rho_2}{\rho_1}, \frac{\mu_2}{\mu_1}, Pr_1), \tag{5}$$

where $Re_{in} \equiv \frac{\rho_2 V_{avg} D_H}{\mu_2}$, $V_{avg}$ is the vapor average velocity, $D_H \equiv \frac{2hw}{(h+w)}$, $Ja \equiv \frac{C_{p1} \cdot \Delta T}{h_{fg}}$, and $Pr_1 \equiv Pr_l \equiv \frac{\mu_1 C_{p1}}{k_1}$. In the experimental data obtained in this report and as described

earlier through Fig. 2.4, properties $\frac{\rho_2}{\rho_1}$, $\frac{\mu_2}{\mu_1}$, and $Pr_1$ may be assumed to vary only in a very small cubical neighborhood of a representative point identified by $\frac{\rho_2}{\rho_1} \cong \frac{\rho_2}{\rho_1}^* \cong$ 0.01157, $\frac{\mu_2}{\mu_1} \cong \frac{\mu_2}{\mu_1}^* \cong 0.01083$, and $Pr_1 \cong Pr_1^* \cong 9.472$. Under the above approximation assumption (which can be relaxed in computational-modeling), eq. (5) reduces to a characterization of the type

$$\frac{X_A}{h} = \text{function } (Re_{in}, Ja), \tag{6}$$

where $Re_{in}$ and Ja respectively represent the non-dimensional form of $\dot{M}_{in}$ and $\Delta T$ appearing in eq. (3).

# 4. Results and Discussions

## 4.1 Experimental Data

The experimental data set corresponding to sets $S_1$, $S_2$, and $S_3$ described in section 2.4.2, are in Tables 4.1and 4.2 below. Table 4.1 gives the run conditions which, in conjunction with fluid properties (FC-72) available from 3M Corporation, are used to define the physical and non-dimensional variables in eq. (3) and eq. (6). Table 4.2 provides the raw data and the error associated with the measured values of the length of the annular regime, $X_A$.

The actual wall temperature variations, $T_w(x)$, for the cases in Table 4.1 are shown in Fig. 4.1. Using the definition in eq. (1), the cooling condition profile, $\theta(x/X_A)$, is shown in Fig. 4.2. The modeled value of $\theta(x/X_A)$, shown as the dashed red line in Fig. 4.2, represents our "assumed" form of $\theta(x/X_A)$ which does not vary from case to case over the data set in Tables 4.1 and 4.2.

**Table 4.1**
The data set for quasi-steady of FC-72 (see Fig. 2.4)

| Name | $X_A$(cm) | $\dot{M}_{in}$ (g/s) | $\Delta T$ (°C) | $p_{in}$(kPa) | $\overline{T}_w$ (°C) | $q''_{w\|avg@x=40cm}$ (W/cm$^2$) |
|---|---|---|---|---|---|---|
| S1C1 | 50 | 0.716563 | 16.437 | 104.876 | 41.200 | 0.261725059 |
| S1C2 | 45 | 0.708276 | 16.272 | 109.930 | 42.270 | 0.254545277 |
| S1C3 | 41 | 0.699952 | 17.531 | 114.930 | 42.776 | 0.282779391 |
| S1C4 | 40 | 0.729967 | 18.635 | 120.712 | 43.250 | 0.1800877 |
| S1C5 | 36 | 0.698367 | 18.5 | 124.839 | 43.365 | 0.287590615 |
| S1C6 | 32 | 0.698904 | 19.587 | 129.777 | 43.792 | 0.293088801 |
| S1C7 | 32 | 0.700605 | 22.977 | 134.727 | 38.556 | 0.281872234 |
| S1C8 | 27 | 0.705494 | 18.442 | 139.661 | 46.322 | 0.284068598 |
| S1C9 | 27 | 0.697347 | 18.49 | 144.647 | 47.377 | 0.301519535 |
| S1C10 | 25 | 0.706696 | 18.792 | 149.673 | 48.611 | 0.325850634 |
| S1C11 | 23 | 0.702154 | 19.907 | 154.698 | 49.072 | 0.342047012 |
| S1C12 | 23 | 0.702030 | 20.843 | 159.644 | 49.083 | 0.303872669 |
| S1C13 | 20 | 0.704796 | 21.947 | 164.567 | 50.076 | 0.336560553 |
| S1C14 | 15 | 0.706115 | - | 169.520 | 54.111 | 0.334647391 |
| S1C15 | 15 | 0.706458 | - | 174.521 | 55.086 | 0.365126468 |
| S1C16 | 15 | 0.702714 | - | 179.504 | 55.702 | 0.345998731 |
| S1C17 | 15 | 0.705748 | - | 179.490 | 54.896 | 0.407531308 |

Table 4.1 (continued)

| Name | $X_A$(cm) | $\dot{M}_{in}$ (g/s) | ΔT (°C) | $p_{in}$(kPa) | $\overline{T}_w$ (°C) | $q''_{w\|avg@x=40cm}$ (W/cm$^2$) |
|---|---|---|---|---|---|---|
| S1C18 | 15 | 0.703524 | - | 182.472 | 55.166 | 0.405972324 |
| S1C19 | 15 | 0.702140 | - | 184.455 | 55.268 | 0.409355732 |
| S1C20 | 15 | 0.702661 | - | 186.448 | 55.349 | 0.387441345 |
| S1C21 | 15 | 0.701722 | - | 189.445 | 55.485 | 0.396587893 |
| S1C22 | 50 | 0.708309 | - | 99.9833 | 40.657 | 0.24086962 |
| S1C23 | 53 | 0.699137 | - | 99.8052 | 42.896 | 0.227005727 |
| S1C24 | 59 | 0.699514 | 11.546 | 99.7926 | 44.795 | 0.22381451 |
| S1C25 | 65 | 0.699249 | 9.4705 | 99.7986 | 46.773 | 0.213781656 |
| S1C26 | 71 | 0.702021 | 7.9485 | 99.9804 | 48.688 | 0.180775608 |
| S1C27 | 90 | 0.700633 | 6.796 | 99.9986 | 49.872 | 0.157149259 |
| S1C28 | 93 | 0.700936 | 6.6294 | 99.9914 | 50.102 | 0.149376825 |
| S1C29 | 95 | 0.698658 | 5.9192 | 99.9871 | 50.574 | 0.115121742 |
| S2C1 | 45 | 0.700635 | 30.02139 | 189.999 | 44.918 | 0.450125407 |
| S2C2 | 10 | 0.602609 | - | 189.718 | 58.138 | 0.502054724 |
| S2C3 | 8 | 0.504345 | - | 189.712 | 60.195 | 0.461387952 |
| S2C4 | 5 | 0.404067 | - | 189.724 | 65.291 | 0.277035516 |
| S2C5 | 0 | 0.331656 | - | 189.999 | 76.561 | 0.230874161 |
| S2C6 | 32 | 1.000774 | 22.68535 | 189.568 | 52.518 | 0.610366856 |
| S2C7 | 42 | 1.500137 | 18.90149 | 189.612 | 57.113 | 0.870935014 |
| S2C8 | 54 | 1.999662 | 15.61418 | 189.630 | 60.275 | 0.85456813 |
| S2C9 | 68 | 2.496707 | 13.49412 | 189.756 | 62.673 | 0.948332332 |
| S2C11 | 81 | 2.703571 | 13.95191 | 189.737 | 63.050 | 0.962713052 |
| S2C12 | 88 | 2.899100 | 12.31798 | 189.697 | 63.972 | 0.960716674 |
| S2C13 | 90 | 3.000205 | 12.47267 | 189.974 | 64.434 | 0.962627344 |
| S2C14 | 99 | 3.299994 | 10.96475 | 189.813 | 64.971 | 0.956735866 |
| S3C2 | 42 | 0.600643 | 17.28447 | 101.033 | 39.060 | 0.231274866 |
| S3C3 | 32 | 0.501371 | 17.08697 | 101.019 | 38.959 | 0.197202204 |
| S3C4 | 27 | 0.400902 | 17.37625 | 101.010 | 37.559 | 0.182198643 |
| S3C5 | 4 | 0.300772 | - | 100.983 | 52.257 | 0.140694521 |
| S3C6 | 48 | 0.701973 | 16.21648 | 101.008 | 39.457 | 0.262068698 |
| S3C7 | 57 | 1.000703 | 13.03246 | 101.047 | 43.054 | 0.401488018 |
| S3C8 | 70 | 1.498692 | 10.43457 | 101.074 | 46.681 | 0.591300125 |
| S3C9 | 88 | 1.599865 | 9.815747 | 101.072 | 46.811 | 0.595705202 |
| S3C10 | 96 | 1.689208 | 9.804532 | 100.997 | 46.885 | 0.59244121 |

**Table 4.2**
Annular Length

| Name | $\overline{X}_A$ (cm) | $\Delta X_{A,max}$ (cm) | $\frac{\Delta X_{A,max}}{\overline{X}_A}$ (%) | $X_A$ from Equation | % Different from actual value |
|---|---|---|---|---|---|
| S1C2 | 45 | 5 | 11.11 | 38.15483 | 15.2114849 |
| S1C3 | 41 | 9 | 21.95 | 34.42335 | 16.04060627 |
| S1C5 | 36 | 4 | 11.11 | 32.02467 | 11.04257672 |
| S1C8 | 27 | 2 | 7.4 | 32.26275 | 19.49165128 |
| S1C9 | 27 | 3 | 11.11 | 32.03125 | 18.63426797 |
| S1C10 | 25 | 4 | 16 | 31.48342 | 25.93366263 |
| S1C11 | 23 | 2 | 8.7 | 29.10042 | 26.52356375 |
| S1C12 | 23 | 4 | 17.4 | 27.37316 | 19.01374253 |
| S1C13 | 20 | 3 | 15 | 25.58898 | 27.94487849 |
| S1C22 | 50 | 0 | 0 | 40.35294 | 19.2941135 |
| S2C6 | 32 | 0 | 0 | 27.39507299 | 14.39039691 |
| S2C7 | 42 | 3 | 7.1 | 39.74922155 | 5.358996321 |
| S2C8 | 54 | 6 | 11.11 | 56.18650033 | 4.049074693 |
| S2C9 | 68 | 8 | 11.76 | 73.24390148 | 7.711619825 |
| S2C11 | 81 | 4 | 4.94 | 71.87265061 | 11.26833258 |
| S2C12 | 88 | 3 | 3.40 | 86.73875131 | 1.433237149 |
| S2C13 | 90 | 1 | 1.11 | 86.25189884 | 4.164556845 |
| S2C14 | 99 | 0 | 0 | 105.5436977 | 5.543697728 |
| S3C2 | 42 | 3 | 6.6 | 33.40265 | 20.4698786 |
| S3C3 | 32 | 8 | 25 | 32.012 | 0.03749814 |
| S3C4 | 27 | 1 | 3.70 | 29.14318 | 7.93769575 |
| S3C6 | 48 | 2 | 4.16 | 38.21964 | 20.3757433 |
| S3C7 | 57 | 2 | 3.50 | 57.25575 | 0.44868856 |
| S3C8 | 70 | 2 | 2.86 | 87.57155 | 25.1022181 |
| S3C9 | 88 | 3 | 3.41 | 96.99628 | 10.2230418 |
| S3C10 | 96 | 4 | 4.17 | 98.84787 | 2.96653213 |

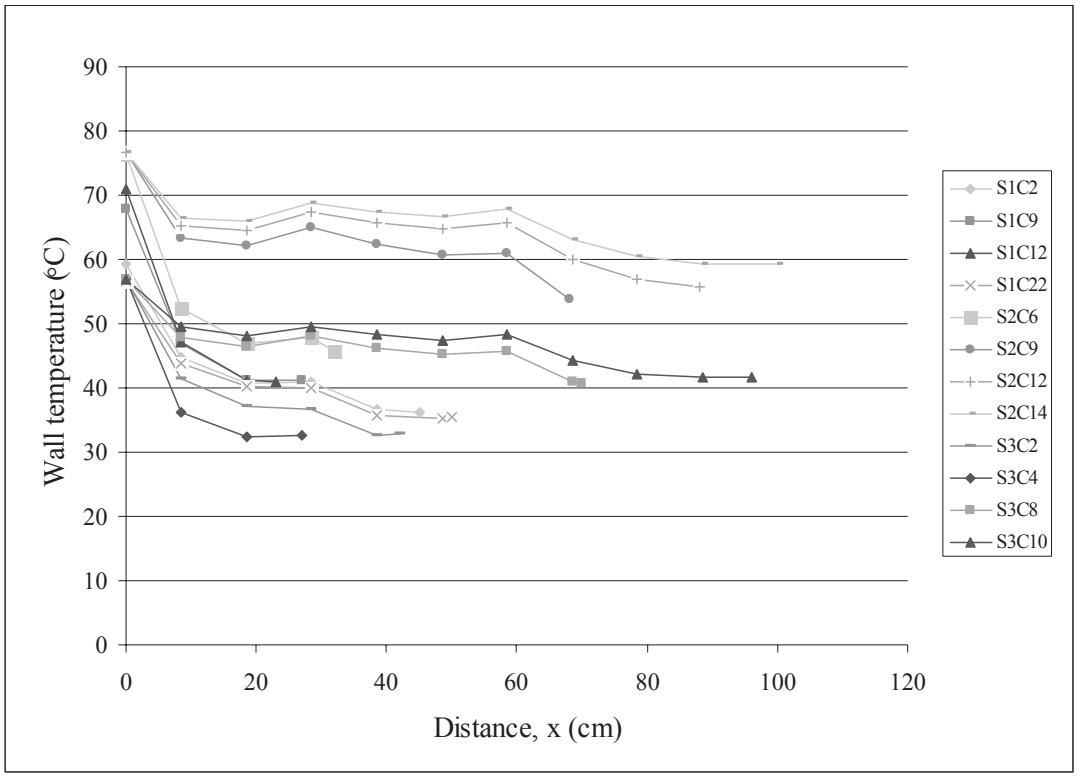


Fig. 4.1: Wall temperature variation ($T_w$)

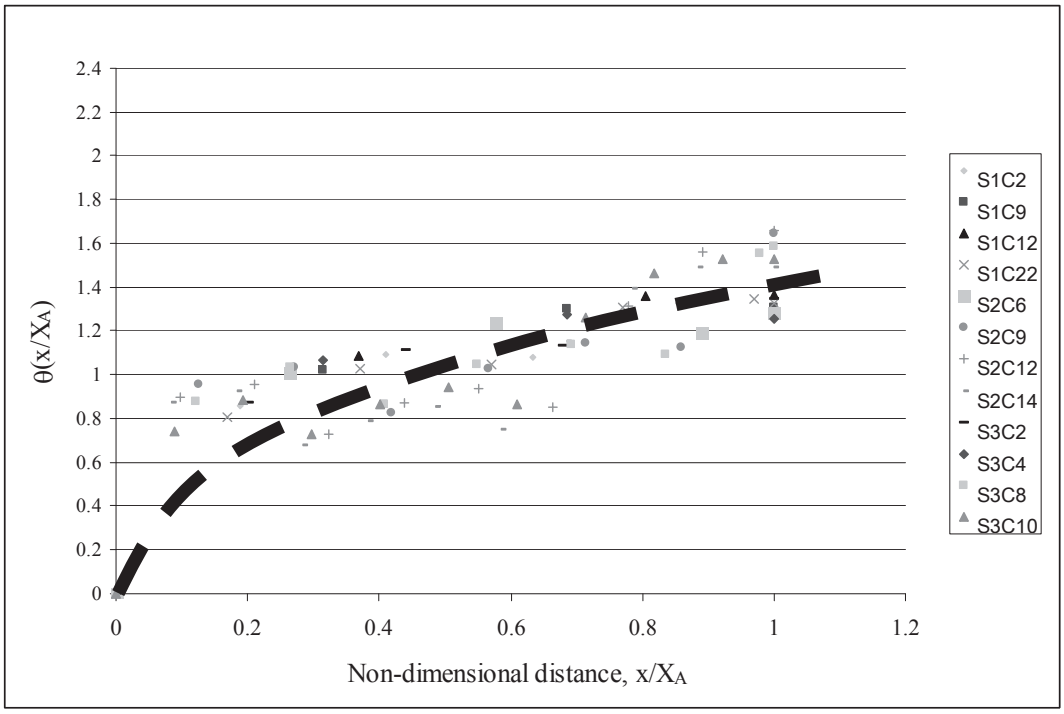


Fig. 4.2: Non-dimension temperature θ(x)

### 4.2 Experiment Results

After collecting data from NI's data acquisition system via a LabView program, most of the data processing was done in Microsoft Excel but some procedures, such as surface fitting for eq. (2), were done with the help of MatLab.

The argument list ($\dot{M}_{in}$ and $\Delta T$) for eq. (2) was varied over the domain shown in Fig. 4.3 (also see Fig. 2.4). The range of variations when considered to be the larger solid rectangular box of Fig. 4.3, are:

$$\left.\begin{aligned} 0.4 \le \dot{M}_{in} \le 3.3 \ \text{(g/s)} \\ 9.8 \le \Delta T \le 22.7 \ (^{\circ}\text{C}) \end{aligned}\right\} \quad (7)$$

A more accurate representation of the experimentally considered data set in Fig. 4.3 is the dashed polygon lying within the solid rectangle of Fig. 4.3.

The experimentally assessed values of $X_A$ for the data set in Fig. 4.3 or eq. (7) were plotted as a 2-D surface.

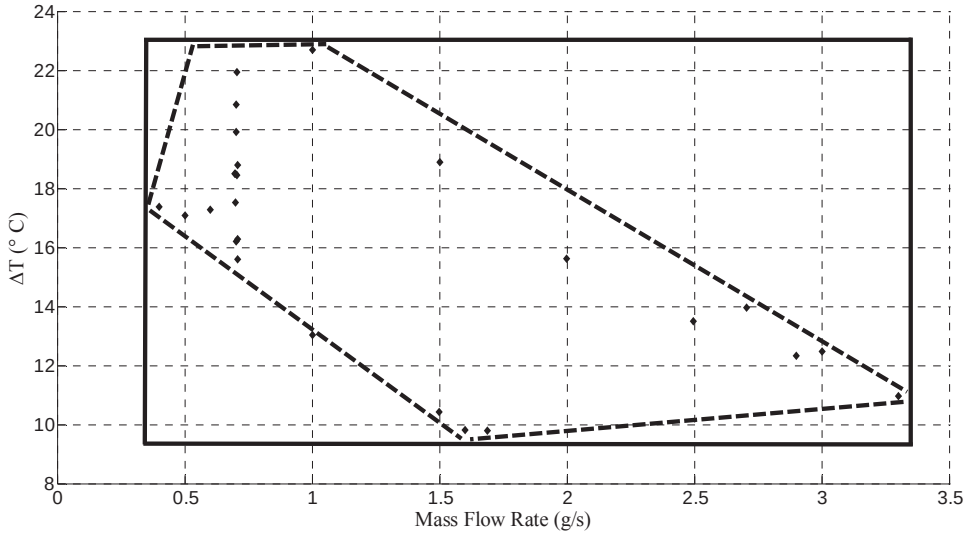


Figure 4.3: The parameter range considered for $\dot{M}_{in}$ and $\Delta T$

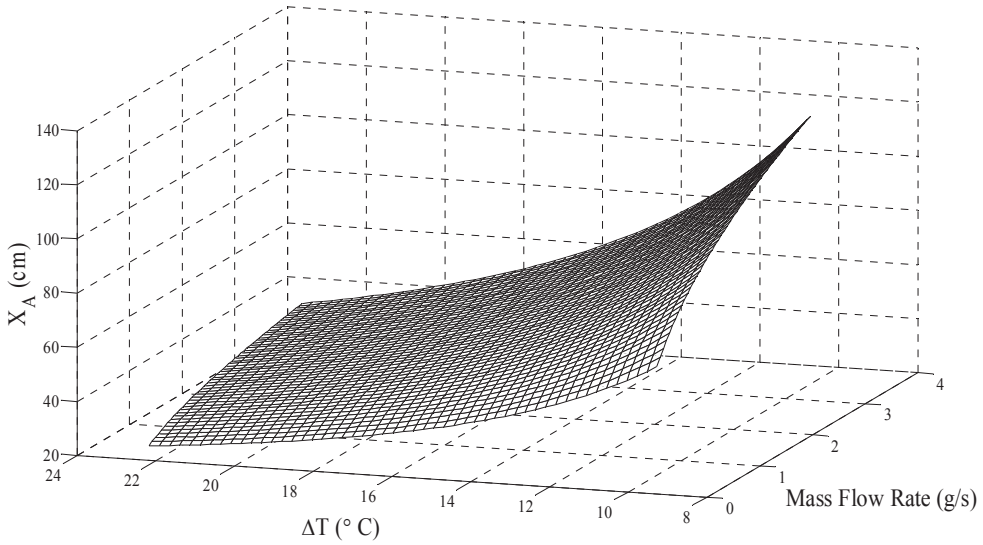


Fig. 4.4: Surface from the annular length equation, eq. 8

To fit the smooth surface to the 3-D data in MatLab, the variables were transformed to a logarithmic scale (i.e. ln $\dot{M}_{in}$ , ln $\Delta T$, and ln $X_A$ were used for the range of data given by eq. (7)). The resulting smooth surface is a *smooth plane* obtained by the least square method. The resulting correlation for the power law surface (shown in raw variables) is shown in Fig. 4.4. The equation for this surface is

$$\left.\begin{aligned} X_A\,(\text{cm}) \cong 1740.63\left[\frac{\text{cm}}{(\text{g/s})^{0.32}(^{\circ}\text{C})^{-1.33}}\right]\cdot \dot{M}_{in}^{0.32}\Delta T^{-1.33} \quad \text{where,} \\ 0.4 \le \dot{M}_{in} \le 3.3 \ \ (\text{g/s}) \\ 9.8 \le \Delta T \le 22.7 \ \ (^{\circ}\text{C}) \end{aligned}\right\} (8)$$

With regard to the non-dimensional version of eq. (3) as given by eq. (6), the data set in Table 4.1 and 4.2 yield slight variations in the values of $\frac{\rho_2}{\rho_1}$, $\frac{\mu_2}{\mu_1}$, and $Pr_1$. These variables and their variations are shown in Fig. 4.5.

Under the above approximation for eq. (5), which leads to eq. (6), the unknown non-dimension function on the right side of eq. (6) is graphically represented (for the data in eq. 9) by Fig. 4.6. The analytical power law fit for the surface in Fig. 4.6 is given by:

$$\frac{X_A}{h} \cong 47572.02 Re_{in}^{\ 0.81} Ja^{-7.24}, \text{ where}$$

$$104 \le Re_{in} \le 1034$$

$$3.68 \le Ja \le 4.25 \qquad (9)$$

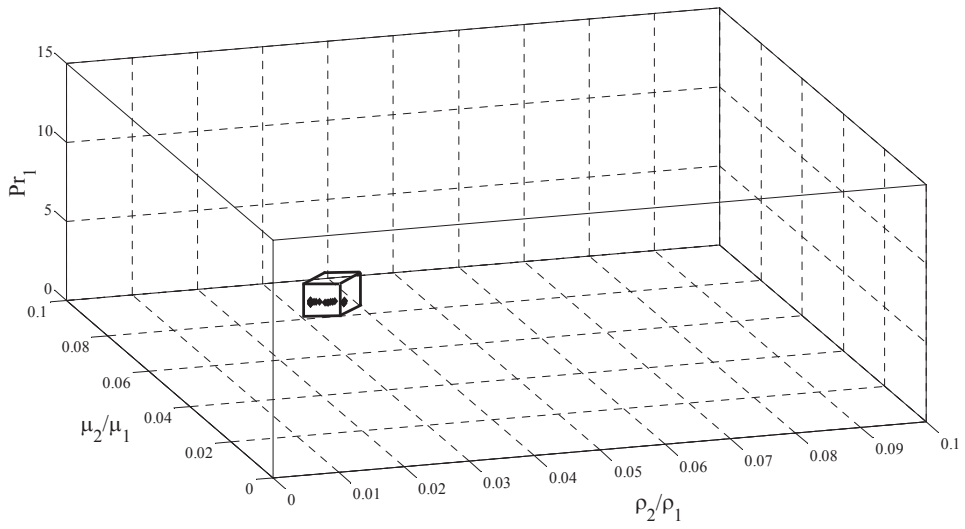


Fig. 4.5: The plot of the variations $\frac{\rho_2}{\rho_1}$, $\frac{\mu_2}{\mu_1}$, and $Pr_1$ for the data given in Table 4.1 and 4.2.

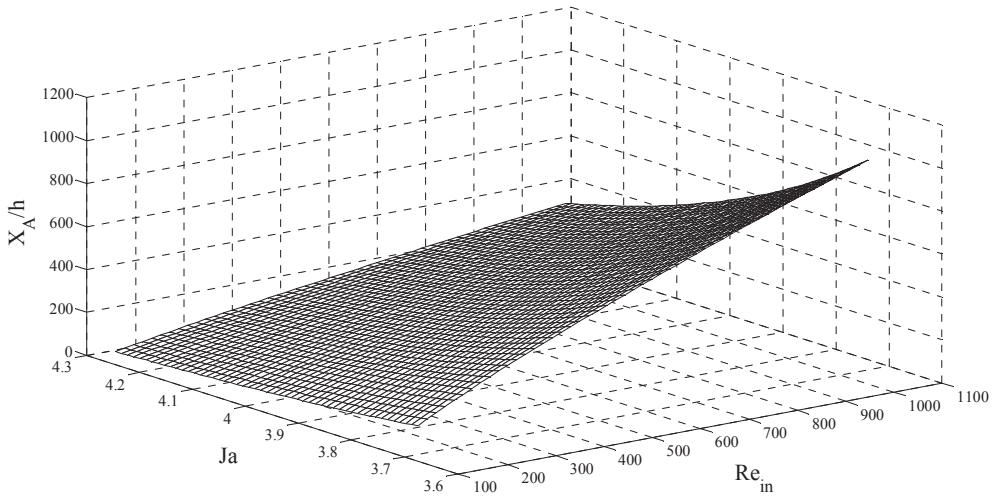


Fig. 4.6: Surface representative for eq. (6).

## 5. Conclusion

The experimental correlation for the length of the annular regime, as given by eq. (8) and (9), are, to our knowledge, the first experimental characterization of the parameter-space boundary that one needs to know in order to ensure that annular shear/pressure driven condensing flows can be realized within the condenser.

Therefore, this report is helpful in the design of new condensers which requires annular regime flows over most of the length of the condenser. This is needed for high heat flux and high system stability purposes, provided the system design allows only partial condensation in the condenser. Condenser and system designs which involve partial condensation flows (with recirculating vapor) have been proposed by our group.

Though the experimental data and the correlation are for a single fluid and a limited range of operation conditions, its true value lies in providing a test for similar results that our group is trying to obtain by computation and simulations. Reasonable agreements with these experiments (particularly with regard to annular zone heat-flux data given in Table 4.1), have already been achieved by the modeling group at Michigan Tech. Once an agreement between the reported results on the values of $X_A$ is established, the modeling group's extension of the proposed correlation eq. (8) will cover other fluids and more extended parameter ranges. This will significantly enhance the value of the results reported in eqs. (8) and (9).

REFERENCES

Cavallini A, Zechchin R. 1971. High velocity condensation of R-11 vapors inside vertical tubes. Heat Transfer in Refrigeration. Proc. IIR Commision 2, Tronheim, Norway. 385-396.

Cavallini A, Smith JR, Zechchin R. 1974. A Dimensionless Correlation for Heat Transfer in Forced Convection Condensation. 6th International Heat Transfer Conference, Tokyo, Japan. 3:309-313.

Goodykoontz JH, Dorsch RG. 1966. Local heat transfer coefficients for condensation of steam vertical down flow within a 5/8-inch diameter tube. NASA TN D-3326.

Kivisalu M, Gorgitrattanagul P, Mitra S, Naik R, Narain A. 2011. Prediction and Control of Internal Condensing Flows in the Experimental Context of their Inlet Condition Sensitivities. Journal of Microgravity Science and Technology. MGST318R1.

Kivisalu M, Gorgitrattanagul N, Mitra S, Naik R, Narain A. 2011. Shear/Pressure Driven Internal Condensing Flows and Their Sensitivity to Inlet Pressure Fluctuations. International Mechanical Engineering Congress and Exposition. "in press"

Kurita J, Kivisalu M, Mitra S, Naik R, Narain A. 2011. Experimental Results on Gravity Driven Fully Condensing Flows in Vertical Tubes, their Agreement with Theory, and their Differences with Shear Driven Flow's Boundary Condition Sensitivities. International Journal of Heat and Mass Transfer. 54:2932-2951.

Mitra S, Narain A, Naik R, Kulkarni SD. 2011. A Quasi One-Dimensional Simulation Method and its Results for Steady Annular/Stratified Shear and Gravity Driven Condensing Flows. International Journal of Heat and Mass Transfer. 54:3761-3776.

Munson BR, Young DF, Okiishi TH, Huebsch WW. 2009. Fundamentals of Fluid Mechanics. 6th ed. United State of America: John Wiley & Sons, Inc.

Narain A, Liang Q, Yu G, Wang X. 2004. Direct Computational Simulations for Internal Condensing Flows and Results on Attainability/Stability of Steady Solutions, Their Intrinsic Waviness, and Their Noise-Sensitivity. Journal of Applied Mechanics. 71:69-88.

Shah MM. 1979. A General Correlation for Heat Transfer during Film Condensation inside Pipes. International Journal of Heat and Mass Transfer 22:547-556.